JOURNAL OF BIOMOLECULAR STRUCTURE AND DYNAMICS
https://doi.org/10.1080/07391102.2020.1764868

Potential inhibitors of coronavirus 3-chymotrypsin-like protease ($3CL^{pro}$): an *in silico* screening of alkaloids and terpenoids from African medicinal plants

Gideon A. Gyebi[a], Olalekan B. Ogunro[b], Adegbenro P. Adegunloye[c], Oludare M. Ogunyemi[a] and Saheed O. Afolabi[d]

[a]Department of Biological Sciences, Salem University, Lokoja, Nigeria; [b]Department of Biological Sciences, KolaDaisi University, Ibadan, Nigeria; [c]Department of Biochemistry, Faculty of Life Sciences, University of Ilorin, Ilorin, Nigeria; [d]Department of Pharmacology and Therapeutics, Faculty of Basic Medical Sciences, University of Ilorin, Ilorin, Nigeria

Communicated by Ramaswamy H. Sarma

ABSTRACT

The novel coronavirus disease 2019 (COVID-19) caused by SARS-COV-2 has raised myriad of global concerns. There is currently no FDA approved antiviral strategy to alleviate the disease burden. The conserved 3-chymotrypsin-like protease ($3CL^{pro}$), which controls coronavirus replication is a promising drug target for combating the coronavirus infection. This study screens some African plants derived alkaloids and terpenoids as potential inhibitors of coronavirus $3CL^{pro}$ using *in silico* approach. Bioactive alkaloids (62) and terpenoids (100) of plants native to Africa were docked to the $3CL^{pro}$ of the novel SARS-CoV-2. The top twenty alkaloids and terpenoids with high binding affinities to the SARS-CoV-2 $3CL^{pro}$ were further docked to the $3CL^{pro}$ of SARS-CoV and MERS-CoV. The docking scores were compared with $3CL^{pro}$-referenced inhibitors (Lopinavir and Ritonavir). The top docked compounds were further subjected to ADEM/Tox and Lipinski filtering analyses for drug-likeness prediction analysis. This ligand-protein interaction study revealed that more than half of the top twenty alkaloids and terpenoids interacted favourably with the coronaviruses $3CL^{pro}$, and had binding affinities that surpassed that of lopinavir and ritonavir. Also, a highly defined hit-list of seven compounds (10-Hydroxyusambarensine, Cryptoquindoline, 6-Oxoisoiguesterin, 22-Hydroxyhopan-3-one, Cryptospirolepine, Isoiguesterin and 20-*Epi*bryonolic acid) were identified. Furthermore, four non-toxic, druggable plant derived alkaloids (10-Hydroxyusambarensine, and Cryptoquindoline) and terpenoids (6-Oxoisoiguesterin and 22-Hydroxyhopan-3-one), that bind to the receptor-binding site and catalytic dyad of SARS-CoV-2 $3CL^{pro}$ were identified from the predictive ADME/tox and Lipinski filter analysis. However, further experimental analyses are required for developing these possible leads into natural anti-COVID-19 therapeutic agents for combating the pandemic.

ARTICLE HISTORY
Received 22 April 2020
Accepted 28 April 2020

KEYWORDS
COVID-19; SARS-CoV-2; coronavirus 3CLpro; natural product; molecular docking

1. Introduction

The novel coronavirus called severe acute respiratory syndrome coronavirus 2 (SARS-CoV-2) is responsible for the pandemic officially called coronavirus disease 2019 (COVID-19), and was first identified in December 2019 in Wuhan, China from cluster of patients(Zhu et al., 2020). This is somewhat different from the world-wide endemic human coronaviruses HCoV-229E, HCoV-NL63, HCoV-HKU1, and HCoV-OC43; the zoonotic Middle East respiratory syndrome coronavirus (MERS-CoV); and the severe acute respiratory syndrome coronavirus (SARS-CoV) known with high mortality (Who, 2020). People infected with SARS-CoV-2 have shown symptoms including fever, cough, apnea, dyspnea and respiratory symptoms (Cascella et al., 2020). Unfortunately, there is currently no specific medicine or treatment for COVID-19 (Wu et al., 2020). From the first documented case, COVID-19 has since spread to over 190 countries and territories in the world including many African countries like Algeria, Egypt, Tunisia, Morocco, Nigeria, South Africa, and Senegal where hundreds of millions of people live with HIV/AIDS, tuberculosis or malaria (Dong et al., 2020). The genome of SARS-CoV-2 is about 80% identical and evolutionarily related to the beta-coronavirus responsible for the severe acute respiratory syndrome (SARS), which caused global outbreak in 2003 (Chen et al., 2020; Wang et al., 2020; Wu et al., 2020).

An overarching therapeutic enquiry is to rapidly identify and develop antiviral agents, as no drug nor vaccineis currently available to contain this on-going pandemic. In this direction, molecular docking and other computation techniques have proved valuable in the initial large-scale screening of several natural compounds and small molecules that directly inhibit important target proteins. Based on the available knowledge of the SARS-CoV-2 and closely related coronaviruses, reports on virtual screening of existing antiviral drugs (Boopathi et al., 2020 {Muralidharan et al., 2020), available databases (Khan et al., 2020) and natural agents (Aanouz et al., 2020; Elfiky & Azzam, 2020; Pant et al., 2020) against emerging targets such as viral spike proteins (Hasan et al., 2020), envelop protein (Gupta et al., 2020), protease (Khan

CONTACT Gideon A. Gyebi gideonagyebi@gmail.com Department of Biological Sciences, Salem University, Lokoja, Nigeria

et al., 2020), nucleocapsid protein (Sarma et al., 2020), 2′-O-ribose methyltransferase (Khan et al., 2020) and 3CL hydrolase (Elmezayen et al., 2020) is rapidly emerging.

The 3-chymotrypsin-like protease ($3CL^{pro}$) also known as main protease (M^{pro}), and the papain-like protease (PL^{pro}) of the virus are two proteases vital to transcription and replication of the proteins the viral genome encodes because of their peculiarity to split the two translated polyproteins (PP1a and PP1ab) into separate functional constituents (Chen et al., 2020). Therefore, the $3CL^{pro}$ is considered to be a promising drug target and a lot of efforts have been committed to its study because of its key role in the replication cycle of the virus (Wang et al., 2020). The $3CL^{pro}$ is responsible for the catalytic cleavage of 11 conserved sites in polyprotein 1ab (PP1ab) and 1a (PP1a) containing a large hydrophobic residue, a glutamine, and a small aliphatic amino acid residue (Anand et al., 2003). The structure and catalytic mechanism of $3CL^{pro}$ makes it a selective target for drug development hence providing possible leads.

Some natural compounds and their derivatives that possess anti-inflammatory and anti-virus effects exhibit high binding affinity to $3CL^{pro}$ (Wu et al., 2020). Likewise, alkaloids and terpenoids, from African plants, with documented antiviral, antimicrobial, antimalarial, antifungal, antileishmanial (Amoa Onguéné et al., 2013; Ndhlala et al., 2013; Osafo et al., 2017; Setzer et al., 2001) properties may inhibit the $3CL^{pro}$ of SARS-CoV-2. This could also buttress reports that some patients with COVID-19 showed improvement when treated with hydroxychloroquine, an antimalarial drug (Wang et al., 2020; Wu et al., 2020)

The 3C-like cleavage sites on the polyproteins of coronaviruses are highly conserved, and their sequence and substrate specificities are identical i.e. SARS-CoV-2, MERS-CoV and SARS-CoV (Chen et al., 2020). This sequential similarity provides the basis for comparing SARS-CoV-2 with its previous counterpart leading to the identification of compounds with potentials to control or inhibit the replication of SARS-CoV-2. Therefore, identifying compounds with inhibitory capacity against the replication mechanism of SARS-CoV-2 could serve as breakthrough in the fight against COVID-19. The aim of this study is to establish a molecular model to delineate the possible inhibitory role of alkaloids and terpenoids against the $3CL^{pro}$ of SARS-CoV-2, thereby providing a possible lead target against the novel pandemic coronavirus disease (COVID-19).

2. Materials and methods

2.1. Protein preparation

The crystal structures of coronoviruses $3CL^{pro}$ used in the docking analysis were retrieved from the Protein Databank (http://www.rcsb.org) with their various PDB identification codes [COVID-19 (6lu7) (Souers et al., 2013); SARS-CoV (2duc) (Lessene et al., 2013); MERS-CoV (2yna) (Pelz et al., 2016)]. All the crystal structures of the $3CL^{pro}$ were processed by removing existing ligands and water molecules while missing hydrogen atoms were added according to the amino acid protonation state at pH 7.0 utilizing Autodock version 4.2 program (Scripps Research Institute, La Jolla, CA). Thereafter, non-polar hydrogens were merged while polar hydrogens were added to each protein. The process was repeated for each protein and subsequently saved into a dockable pdbqt format for molecular docking.

2.2. Ligand preparation

Bioactive alkaloids (62) and terpenoids (100) from African plants were used in this study.

The Structure Data Format (SDF) structures of the $3CL^{pro}$ reference inhibitors (Lopinavir and Ritonavir), and some of the compounds were retrieved from the PubChem database (www.pubchem.ncbi.nlm.nih.gov), other compounds not present on the database were drawn with chemdraw version 19. All the compounds and inhibitors were converted to mol2 chemical format using Open babel (O'Boyle et al., 2011). The nonpolar hydrogen molecules were merged with the carbons, polar hydrogen charges of the Gasteiger-type were assigned and the internal degrees of freedom and torsions were set to zero. The protein and ligand molecules were further converted to the dockable pdbqt format using Autodock tools.

2.3. Molecular docking

Virtual screening of the coronaviruses $3CL^{pro}$ active regions, and determination of binding affinities of the alkaloids, terpenoids and reference inhibitors were carried out using AutoDock vina 4.2 with full ligand flexibility (Trott & Olson, 2010). The results of the top docked compounds obtained from vina were further validated by BINDSURF (https://bio-hpc.ucam.edu/achilles/) (Sanchez-Linares et al., 2012). Pdbqt form of individual protein and ligands were uploaded, and exhaustive series of docking calculations across the whole protein surface to find the spots with the best binding affinities were performed with vina. After the affinities were calculated, vina clusters the results according to the spatial overlapping of the resulting poses. For each cluster, the pose with the best affinity was taken as the representation of this cluster. The binding affinities of compounds for the selected cluster were recorded. The compounds were then ranked by their affinity. The molecular interactions between proteins and respective ligands with higher binding affinity were viewed using Discovery Studio Visualizer version 16.

2.4. ADMET study

To evaluate the drug-likeness prediction of the top compounds that showed a significant binding affinity for the $3CL^{pro}$ of the of SARS-CoV-2, they were subjected to Lipinski filter in which an orally bio-active drug is expected not to violate more than one of the criteria for drug-likeness namely: cLogP, hydrogen donor and acceptor molecular mass, and molar refractive index (Nickel et al., 2014). The predicted Absorption Distribution Metabolism, Excretion and toxicity (ADME/tox) study were analyzed using the SuperPred webserver (http://lmmd.ecust.edu.cn:8000/) which is reported as an important tool in drug discovery (Cheng et al., 2012). The SuperPred webserver was employed for predicting

Table 1. Binding affinities of reference compounds (ritonavir and lopinavir) and top 20 bioactive alkaloids from African plants to the 3CL^{pro} of coronaviruses.

S/No	Bioactive Compounds	Class of compound	Plant species (Family)	SARS-Cov-2	SARS-CoV	MERS-CoV
	Ritonavir			−6.8	−6.6	−7.9
	Lopinavir			−8.3	−7.2	−5.6
1	10-Hydroxyusambarensine	Indole alkaloids	*Strychnos usambarensis* (Loganiaceae)	**−10.0**	**−10.1**	−8.5
2	Cryptoquindoline	Cryptolepines	Cryptolepis sanguinolenta (Periplocaceae)	**−9.7**	−9.3	**−9.9**
3	Cryptospirolepine	Cryptolepines	Cryptolepis sanguinolenta (Periplocaceae)	−9.2	**−10.5**	**−10.9**
4	Chrysopentamine	Indole alkaloids	*Strychnos usambarensis* (Loganiaceae)	−8.5	−8.9	−9.0
5	Isocryptolepine	Cryptolepines	Cryptolepis sanguinolenta (Periplocaceae)	−8.5	−6.7	−7.4
6	Strychnopentamine	Indole alkaloids	*Strychnos usambarensis* (Loganiaceae)	−8.2	−8.9	−9.6
7	Isostrychnopentamine	Indole alkaloids	*Strychnos usambarensis* (Loganiaceae)	−8.1	−9.0	−9.5
8	Normelicopicine	Acridones	Teclea trichocarpa (Rutaceae)	−8.1	−6.8	−6.7
9	Jozipeltine A	Naphthoisoquinolines	Triphyophyllum peltatum,	−8.0		
10	5′-*O*-Demethyl-dioncophylline A	Naphthoisoquinolines	*Triphyophyllum peltatum* (Dioncophyllaceae)	−8.0	−7.8	−8.1
11	Dioncophylline C	Naphthoisoquinolines	*Triphyophyllum peltatum* (Dioncophyllaceae)	−7.9	−8.7	−7.7
12	Dioncopeltine A	Naphthoisoquinolines	*Triphyophyllum peltatum* (Dioncophyllaceae)	−7.8	−7.7	−7.9
13	Liriodenine	Indole alkaloids	*Glossocalyx brevipes* (Siparunaceae)	−7.6	−7.8	−8.1
14	5,6-Dihydronitidine	Furoquinolines	*Toddalia asiatica* (Rutaceae)	−7.6	−7.0	−8.2
15	Hydroxycryptolepine	Cryptolepines	*Cryptolepis sanguinolenta* (Periplocaceae)	−7.6	−7.0	−7.2
16	Cryptoheptine	Cryptolepines	*Cryptolepis sanguinolenta* (Periplocaceae)	−7.6	−7.1	−8.5
17	Annonidine F	Indole alkaloids	*Monodora angolensis* (Annonaceae)	−7.5	−7.9	−7.8
18	Ancistrotanzanine C	Naphthoisoquinolines	*Ancistrocladus tanzaniensis* (Acistrocladaceae)	−7.5	−7.6	−8.7
19	Fagaronine	Indole alkaloids	*Fagara zanthoxyloides* (Rutaceae)	−7.4	−7.7	−7.3
20	Alstonine	Indole alkaloids	*Fagara zanthoxyloides* (Rutaceae)	−7.4	−7.4	−8.1

Compounds having the highest binding affinity for the corresponding proteins are the ones indicated in bold values.

important descriptors of drug-likeness. The SDF file and canonical SMILES of the compounds were downloaded from PubChem Database or copied from ChemDraw to calculate ADMET properties using default parameters.

3. Results and discussion

The result of the binding energy from the docking analysis of bioactive alkaloids (62) and terpenoids (100) to 3-Chymotrypsin-like protease (3CL^{pro}) of the novel SARS-CoV-2 is represented in (supplementary material).

The alkaloids and terpenoids with more negative binding energy values have higher binding affinities for the specific 3CL^{pro} protein, and were ranked higher. The twenty alkaloids and terpenoids with best binding affinities to 3CL^{pro} of SARS-CoV-2, along with their binding affinities to 3CL^{pro} of SARS-CoV and MERS-CoV are presented in Tables 1 and 2.

The results from this study revealed that lopinavir and ritonavir, the reference inhibitors, had a binding affinity of −8.3 and −6.8 Kcal/mol, respectively, for 3CL^{pro} of SARS-CoV-2 (Table 1). The binding affinity of lopinavir and ritonavir for 3CL^{pro} of SARS-CoV was −7.2 and −6.6 Kcal/mol, respectively, while for 3CL^{pro} of MERS-CoV was −5.6 and −7.9 Kcal/mol, respectively (Table 1). It was observed that more than half of the selected top 20 alkaloids and terpenoids had a binding affinity for the 3CL^{pro} of the SARS-coronaviruses that surpassed that of the reference inhibitors (Tables 1 and 2).

The 2 top docked alkaloids to SARS-CoV-2 3CL^{pro} are 10-hydroxyusambarensine (-10.0 kcal mol^{-1}) and cryptoquindoline (−9.7 kcal.mol^{-1}) (Table 1). It was observed that while 10-hydroxyusambarensine was the second top docked compound to the 3CL^{pro} of SARS-CoV, cryptospirolepine had the highest binding affinity to that of SARS-CoV and MERS-CoV (Table 1). The result further showed that 10-hydroxyusambarensine was more selective for SARS-CoV-2 though interacted strongly with the target protein of the other coronavirus, while cryptospirolepine was more selective for the 3CL^{pro} of the MERS-CoV and SARS-CoV respectively (Table 1).

The terpenoids, 6-oxoisoiguesterin (−9.1 kcal.mol^{-1}) a bisnorterpenes, and 22-hydroxyhopan-3-one (−8.6 kcal.mol^{-1}) a pentacyclic triterpenes are the 2 top-docked compounds base on the binding affinities (Table 2). 6-oxoisoiguesterin had the highest binding affinity to the 3CL^{pro} of SARS-CoV-2 while 20-*epi*-isoiguesterinol, isoiguesterin 20-*epi*bryonolic acid were the top docked compounds to 3CL^{pro} of SARS-CoV and MERS-CoV (Table 2). The binding energies of the terpenoids revelaed that 6-oxoisoiguesterin was more selective for the 3CL^{pro} of SARS-CoV and SARS-Cov-2, while isoiguesterin and 20-*epi*bryonolic with the same binding energy (−9.4 kcal.mol^{-1}) interacted more strongly with the 3CL^{pro} of MERS-CoV than that of other coronaviruses.

3.2. Amino acid interaction of selected bioactive alkaloids and terpenoids with 3CL^{pro} of coronaviruses

The interactions of reference inhibitors, and top ranked alkaloids and terpenoids with the amino acids of 3CL^{pro} of coronaviruses are represented in Table 3.

The ligands majorly interacted with the residues through hydrophobic interactions, with few H-bonding above 3.40 Å.

The result obtained from the ligand-protein binding interaction showed that ritonavir was docked into the receptor-binding site and catalytic dyad (Cys-145 and His-41) of SARS-CoV-2 (Figure 2e). Ritonavir interacted via a conventional hydrogen bond to GLY^{143} and GLU^{166}. It further interacted with MET^{165} via a Pi-Sulfur bond and via Pi-Alkyl interaction to PRO^{168} and MET^{49} (Figure 2e). Lopinavir with a considerable higher binding energy (−8.3 kcal.mol^{-1}) than ritonavir did not show significant binding to the catalytic dyad (Cys-145 and His-41) of SARS-CoV-2. It interacted via Hydrogen bond to GLN^{110}, ASP^{153}, and SER^{158}, Pi-Sigma bond to ILE^{106} of Domain II; Pi–Pi Stacking to PHE^{294} of

Table 2. Binding affinities of top 20 bioactive terpenoids from African plants to the 3CL^{pro} of coronaviruses.

S/No	Bioactive Compounds	Class of compound	Plant species (Family)	SARS-Cov-2	SARS-CoV	MERS-Cov
1	6-Oxoisoiguesterin	Bisnorterpenes	Bisnorterpenes	**−9.1**	**−9.5**	−9.3
2	22-Hydroxyhopan-3-one	Pentacyclic triterpenes	Cassia siamea (Fabaceae)	**−8.6**	−8.5	−9.1
3	Isoiguesterin	Bisnorterpenes	Bisnorterpenes	−8.1	−7.4	**−9.4**
4	20-*Epi*-isoiguesterinol	Bisnorterpenes	Bisnorterpenes	−8.1	**−9.2**	−9.3
5	20-*Epi*bryonolic acid	Pentacyclic triterpenes	Cogniauxia podolaena (Cucurbitaceae)	−8.1	−8.6	**−9.4**
6	Oleanolic acid	Pentacyclic triterpenes	Nuxia sphaerocephala (Loganiaceae)	−8.5	−8.6	−8.2
7	3-Oxolupenal (3-oxolup-20(29)-en-30-al)	Pentacyclic triterpenes	Nuxia sphaerocephala (Loganiaceae)	−8.4	−7.8	−8.8
8	2 ,3 ,19 -Trihydroxy-urs-12-20-en-28-oic acid	Pentacyclic triterpenes	Kigelia africana (Bignoniaceae)	−8.4	−9.0	−8.7
9	3-Oxolupenol (30-hydroxylup-20(29)-en-3-one)	Pentacyclic triterpenes	Nuxia sphaerocephala (Loganiaceae)	−8.3	−8.1	−8.9
10	3-*O*-betulinic acid *p*-coumarate	Pentacyclic triterpenes	Baillonella toxisperma (Sapotaceae)	−8.3	−8.2	−8.8
11	Isoiguesterinol	Bisnorterpenes	Bisnorterpenes	−8.1	−8.9	−9.3
12	3- Benzoylhosloppone	Abietane diterpenes	Hoslundia opposita (Lamiaceae)	−8.1	−8.5	−8.7
13	7 -Acetoxy-6,12-dihydroxy-abieta-8, 12-Diene-11,14-dione	Abietane diterpenes	Plectranthus hadiensis (Lamiaceae)	−7.9	−7.7	−6.5
14	Cryptobeilic acid C	Beilshmiedic acid derivatives	Beilschmiedia cryptocaryoides (Lauraceae)	−7.9	−8.3	−7.8
15	3 -Hydroxylupenal (3 -hydroxylup-20(29)-en-30-al)	Pentacyclic triterpenes	Nuxia sphaerocephala (Loganiaceae)	−7.9	−7.8	−9.3
16	3-Friedelanone	Pentacyclic triterpenes	Hypericum lanceolatum (Hypericaceae)	−7.9	−8.7	−8.7
17	6-Acetylswietenolide	Limonoids	Khaya grandifoliola (Meliaceae)	−7.8	−7.6	−7.9
18	11-Hydroxy-19-(4-hydroxy-benzoyloxy)-abieta-5, 7,9(11),13-tetraene-12-one	Abietane diterpenes	Plectranthus purpuratus (Lamiaceae)	−7.8	−8.2	−8.6
19	11-Hydroxy-19-(3,4-dihydroxybenzoyloxy)-abieta-5, 7,9(11),13-tetraene-12-one	Abietane diterpenes	Plectranthus purpuratus (Lamiaceae)	−7.8	−8.5	−8.3
20	3-Hydroxy-20(29)-lupen-28-ol	Pentacyclic triterpenes	Schefflera umbellifera (Araliaceae)	−7.8	−8.3	−8.2

Compounds having the highest binding affinity for the corresponding proteins are the ones indicated in bold values.

Table 3: Interacting amino acid residues of 3CL^{pro} of coronaviruses with the top binding alkaloids and terpenoids from African plants.

Bioactive compound	Coronavirus	Interacted residues	Protein atom involved in H-bonding (BOND DISTANCE)
Ritonavir	SARS-Cov-2	GLU^{166} GLY^{143} MET^{49} MET^{165} PRO^{168}	GLY^{143} (2.97) GLU^{166} (2.97)
Lopinavir		GLN^{110} ASP^{153} SER^{158} ILE^{106} VAL^{104} PHE^{294} VAL^{297} PRO^{293} VAL^{202} ILE^{249}	GLN^{110} (2.11) ASP^{153} (2.80) SER^{158}(3.09)
10 -Hydroxyusambarensine		GLN^{189} TYR^{54} MET^{49} MET^{165} HIS^{163} CYS^{145} GLU^{166} PRO^{168}	GLN^{189} (2.97)
Cryptoquindoline		CYS^{148} MET^{49} MET^{165}	
6-Oxoisoiguesterin		GLN^{189} MET^{49} MET^{165} HIS^{41} CYS^{145}	GLN^{189} (2.75)
22-Hydroxyhopan-3-one		LYS^{137} LEU^{275} LEU^{287} LEU^{286} TYR^{239}	LYS^{137} (3.16)
10-Hydroxyusambarensine	SARS-CoV	PHE^{294} LEU^{202} PRO^{293} VAL^{104} ASP^{153}	
Cryptospirolepine		MET^{49} GLU^{47} CYS^{145}	
6-Oxoisoiguesterin		THR^{292} THR^{111} PRO^{252} PRO^{293} ILE^{294} PHE^{294} VAL^{297}	THR^{292} (3.30) THR^{111} (2.01)
20-*Epi*-isoiguesterinol		THR^{24} THR^{25} ALA^{46} CYS^{145} HIS^{41} MET^{165}	THR^{24} (2.97) THR^{25}(2.92)
Cryptospirolepine	MERS-CoV	ASP^{294} SER^{114} ALA^{113} THR^{154} ASP^{295} MET^{298}	ASP^{294}
Cryptoquindoline		ASP^{294} ASP^{295} MET^{298}SER^{114} ALA^{113} THR^{154}	
Isoiguesterin		ASP^{294} THR^{292} ALA^{113} PRO^{293} LYS^{110}HIS^{135} VAL^{246} PRO^{111} CYS^{203} ILE^{205}	ASP^{294} (2.35)THR^{292} (3.08)
20-*Epi*bryonolic acid		ASP^{294} CYS^{203} SER^{250} PRO^{293} ILE^{205}VAL^{246}	ASP^{294} (2.94) CYS^{203} (2.56) SER^{250} (2.99)

Domain III; Amide-Pi Stacking to PRO^{293} of Domain III; Alkyl and Pi-Alkyl to the other residues (Table 3, Figure 2f).

10-Hydroxyusambarensine the topmost docked compound to the 3CL^{pro} of SARS-CoV-2 interacted via a conventional hydrogen bond to the GLN^{189} residue a carbon-hydrogen bond to GLN^{166} and CYS^{145}, a Pi-Sulfor to MET^{165}, a Pi-Cation to HIS^{41}, a Pi-Alkyl and Pi-Pi Stacking to other residues (Figure 2a and Table 3) Cryptoquindoline interacted to CYS^{145} in a similar pattern as 10-Hydroxyusambarensine, and via Pi-Alkyl to MET^{49} (Figure 2b). A conventional hydrogen bond was observed between 6-Oxoisoiguesterin and ARG^{189}. 6-Oxoisoiguesterin exhibited similar binding patterns, creating an alkyl and Pi-Alkyl stacking with MET^{49,} MET^{165,} and CYS^{145} (Figure 2c). 22-Hydroxyhopan-3-one interacted via conventional hydrogen bond to LYS^{137} and via Alkyl and Pi-Alkyl to LEU^{275} LEU^{287} LEU^{286} and TYR^{239} (Figure 2d).

Unlike the ligand-protein binding interaction of 10-Hydroxyusambarensine to SARS-CoV-2 3CL^{pro} that targeted the Cys-His catalytic dyad (Cys-145 and His-41) along with the other binding residues, the docking analysis revealed that the SARS-CoV 3CL^{pro} interacted with the same ligand differently. A Pi-Pi and Amide- Pi Stacking was observed between 10-Hydroxyusambarensine, PHE^{294,} and PRO^{293} respectively, it further interacted with VAL^{104} and ASP^{153} of the Domain II (102-184 residues) region of the protease via Pi-Alkyl and Pi-Anion bonds (Figure 4a). Cryptospirolepine interacted via a Carbon Hydrogen, Pi-Donor Hydrogen, and Pi-Alkyl bond to CYS^{145}, GLU^{47}, and MET^{49} respectively (Figure 4b), these residues are implicated in the binding of a substrate that targeted the Cys-His catalytic dyad (Cys-145 and His-41) of the protein. THR^{292} and THR^{111} of the protein interacted with 6-oxoisoiguesterin via hydrogen bond, while the other residues (Table 3) interacted via hydrophobic bonds to 6-oxoisoiguesterin (figure 4c). The interaction of 20-*epi*-isoiguesterinol to the SARS-CoV 3CL^{pro} revealed a hydrogen bonding to THR^{24} and THR^{25} while hydrophobic interaction was observed between CYS^{145} HIS^{41} MET^{165} and the ligand (Figure 3d). These residues are also conserved for the Cys-His catalytic dyad binding hotspot.

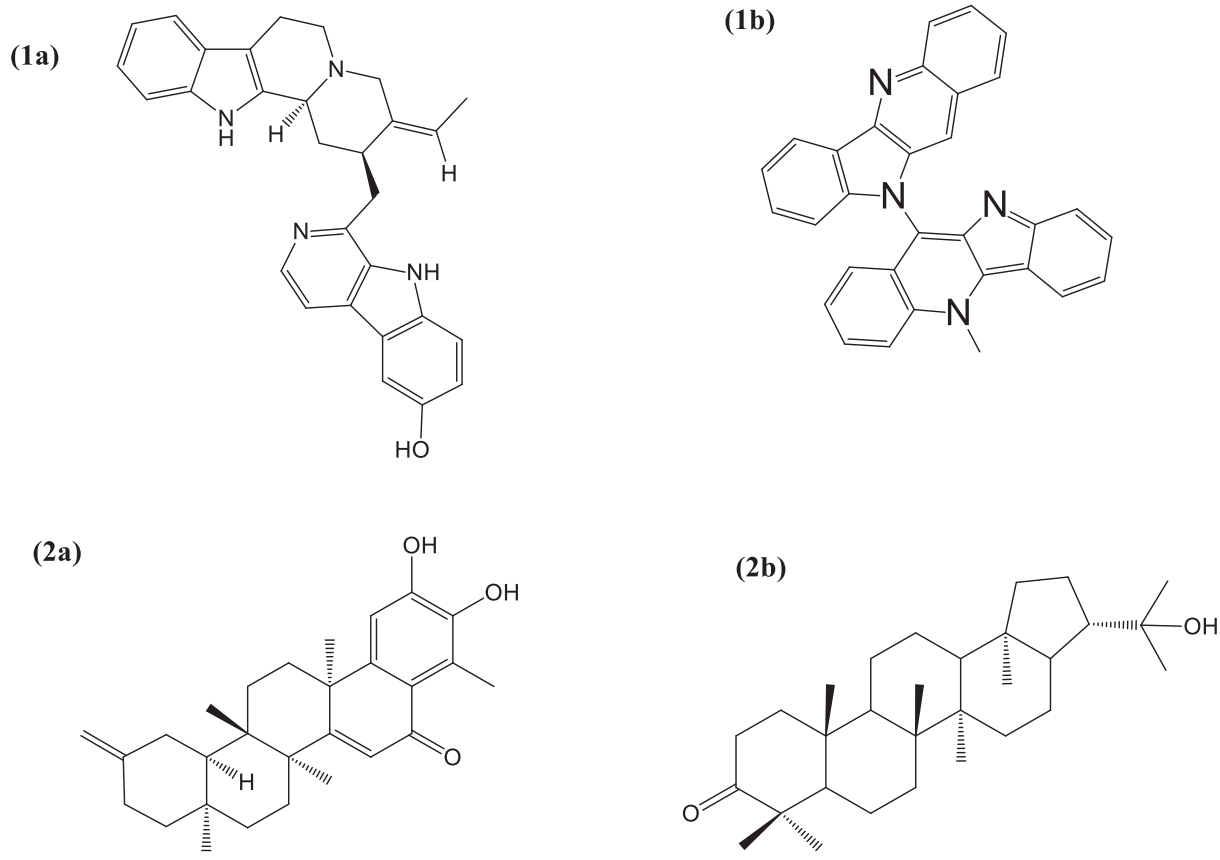

Figure 1. Structure of alkaloids and terpenoids with remarkable binding energy to SARS-CoV-2 $3CL^{pro}$ (1a) 10-Hydroxyusambarensine (1b) Cryptoquindoline (2a) 6-Oxoisoiguesterin (2b) 22-Hydroxyhopan-3-one.

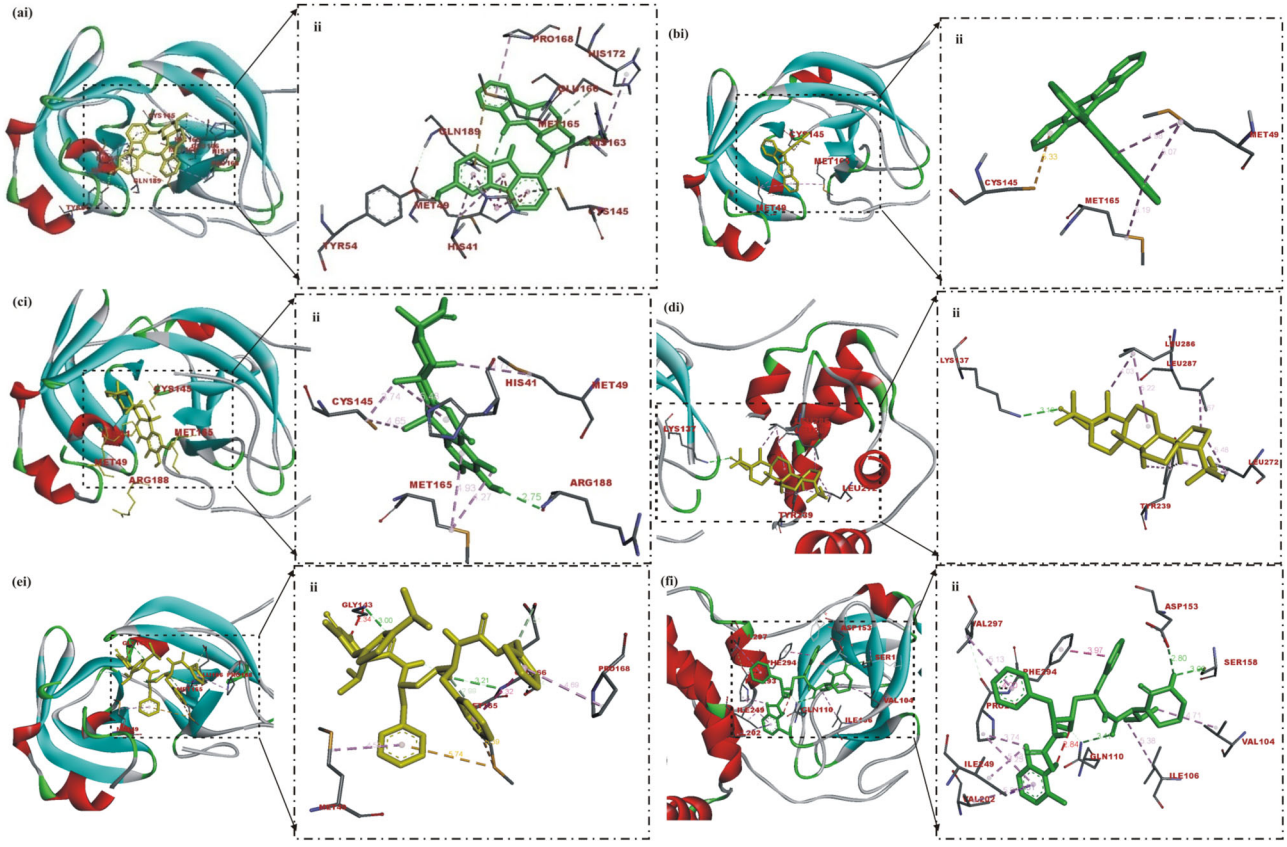

Figure 2. Visualization of SARS-Cov-2 $3CL^{pro}$ amino acids interactions with ligands (a) 10-Hydroxyusambarensine (b) Cryptoquindoline (c) 6-Oxoisoiguesterin (d) 22-Hydroxyhopan-3-one (e) Ritonavir (f) Lopinavir; (i) Cartoon representation, showing binding conformation (ii) interactions view with important residues.

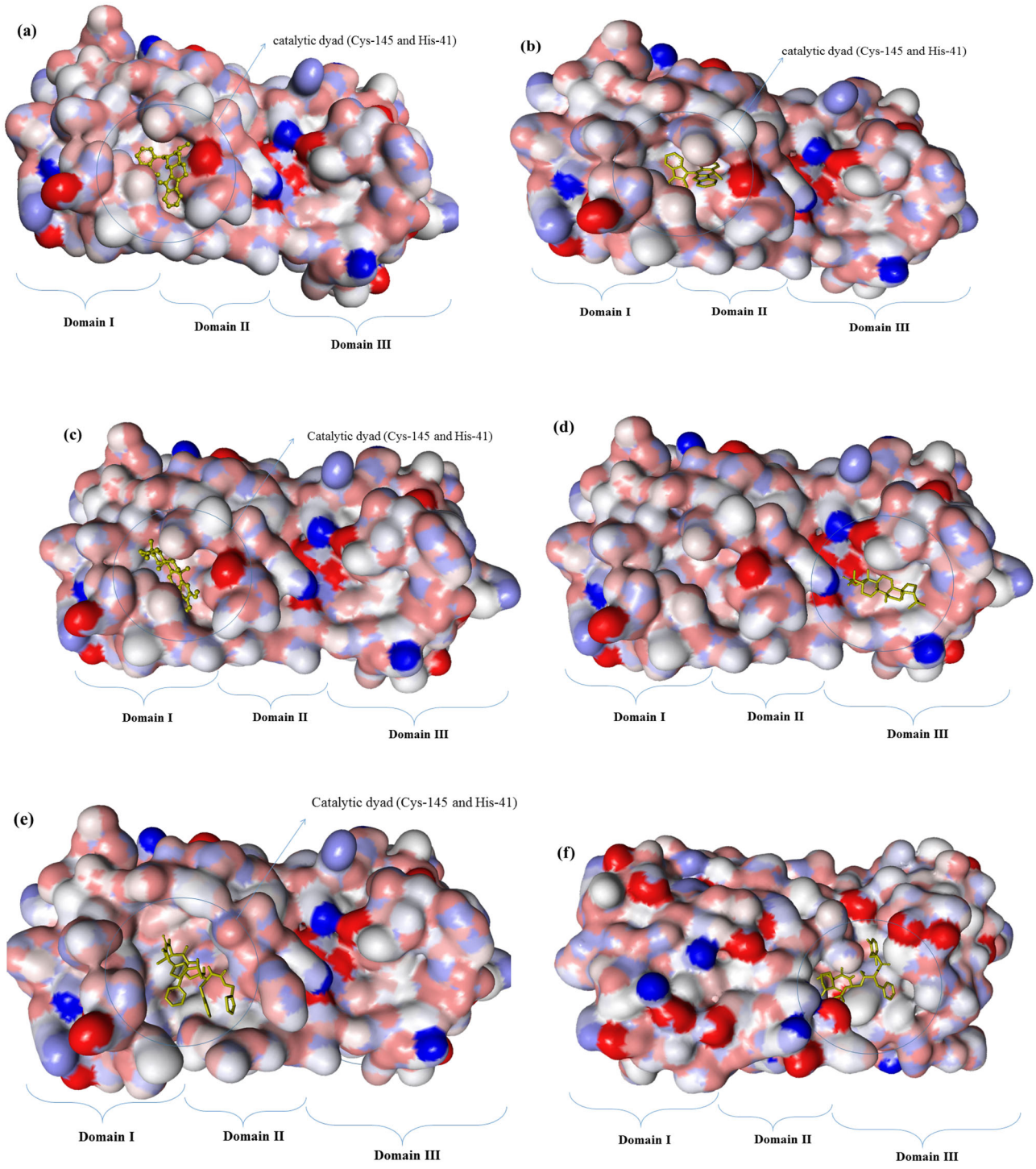

Figure 3. Surface view of ligand in binding cavity of SARS-Cov-2 $3CL^{pro}$ (a) 10-Hydroxyusambarensine (b) Cryptoquindoline (c) 6-Oxoisoiguesterin (d) 22-Hydroxyhopan-3-one (e) Ritonavir (f) Lopinavir.

Cryptospirolepine, cryptoquindoline, isoiguesterin and 20-*epi*bryonolic acid interacted with the MERS-CoV $3CL^{pro}$ in a conservative manner that is different from the other two coronaviruses. The predominate residue involved in the binding processes was outside the Domain I and II of the protein. A hydrogen bond was observed between cryptospirolepine/isoiguesterin/20-*epi*bryonolic acid and ASP^{294} while an extra hydrogen bond interaction with SER^{250} in the case of the latter was also observed (Figure 5 a–c). Cryptospirolepine/cryptoquindoline interacted via hydrophobic (Pi-Sulfur, Pi-Anaion, Pi-Alkyl, and Pi-Donor Hydrogen bonds) to $MET^{298}ASP^{294}$ ALA^{113}, $SER^{114,}$ and THR^{154}, respectively (Figure 5d).

From the results obtained in this study, 7 compounds (10-hydroxyusambarensine, cryptoquindoline, 6-oxoisoiguesterin, 22-hydroxyhopan-3-one, cryptospirolepine, isoiguesterin, 20-*epi*bryonolic acid) with a remarkable inhibitory tendency towards the SARS-coronavirus were identified from plant-

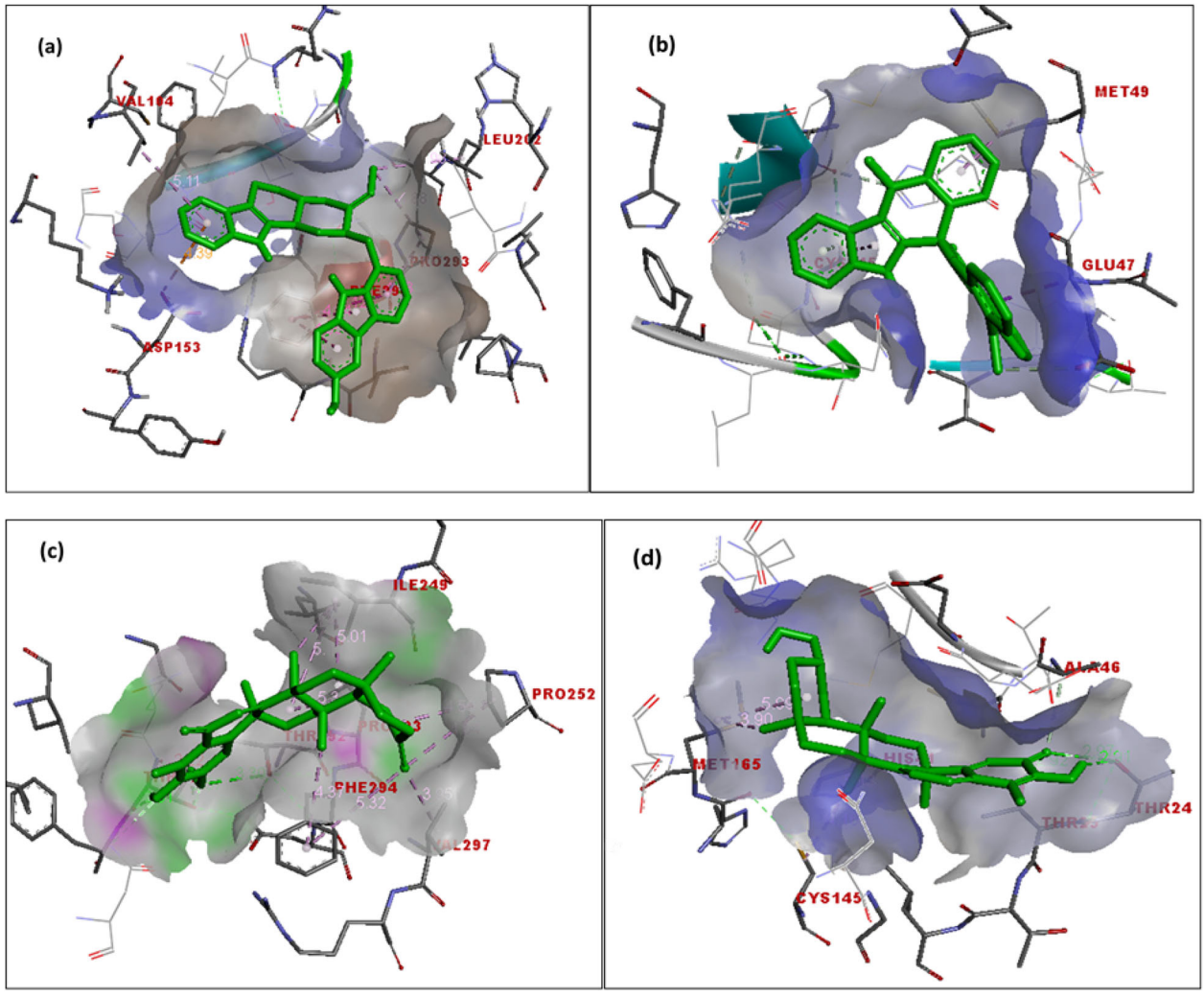

Figure 4. Visualization of SARS-Cov 3CL^{pro} amino acids interactions with ligands (a) 10-Hydroxyusambarensine (b) Cryptospirolepine (c) 6-Oxoisoiguesterin (d) 20-*Epi*-isoiguesterinol.

derived alkaloids and terpenoids. 10-hydroxyusambarensine, cryptoquindoline, 6-oxoisoiguesterin, cryptospirolepine, and 20-*epi*-isoiguesterinol were docked into the Cys-His catalytic dyad of the coronaviruses 3CL^{pro} in a similar pattern as ritonavir, while the rest compounds interacted with the amino residues in the cleft of Domain III of the protein.

3.3. Revalidation of docking scores

The result of the top docked compounds that were obtained from the docking analysis using vina was further revalidated by the docking scores from BINDSURF analysis. The results from Bindsurf analysis was similar to that of vina in most cases the ligand had the same binding affinities with respective proteins as presented, only few differ with the range of ± 2 Kcal/mol. All the Ligands were docked into cavities as revealed by Vina. The ligands exhibited a similar binding pattern and interacted with similar amino acids as presented by Vina. The additional interactions as presented by BINDSURF analysis are listed in Table 4.

Figure 3 shows that from the 4 top docked compounds to the 3CLpro of SARS-CoV, 3 compounds namely: 10-Hydroxyusambarensine, Cryptoquindoline, 6-Oxoisoiguesterin where further revealed to be docked into the substrate binding cavity (Cys-His catalytic dyad (Cys-145 and His-41)). The binding site coordinate further showed that the 3 compounds were docked into the same cavity as the ritonavir.

3.4. Pharmacokinetic properties of selected alkaloids and terpenoids

The result generated from the Lipinski and ADME/tox filtering analyses are represented in Figure 5 and Table 5.

Four (4) compounds fulfilled the requirement for Lipinski analysis of the rule of-five with corresponding favourable predicted ADME/tox parameters. This includes 2 alkaliods (10-hydroxyusambarensine and cryptoquindoline), and 2 terpenoids (6-oxoisoiguesterin and 22-hydroxyhopan-3-one) (Figure 1). The predicted physiochemical properties for bioavailability of the lead compounds was further represented in Figure 5.

The ADME/tox and pharmacokinetic properties from the filtering analyses suggested four compounds with a high probability of absorption, subcellular distribution, except for AMES toxicity parameter which indicated cryptoquindoline to be toxic at a probability of 0.89. All the four compounds

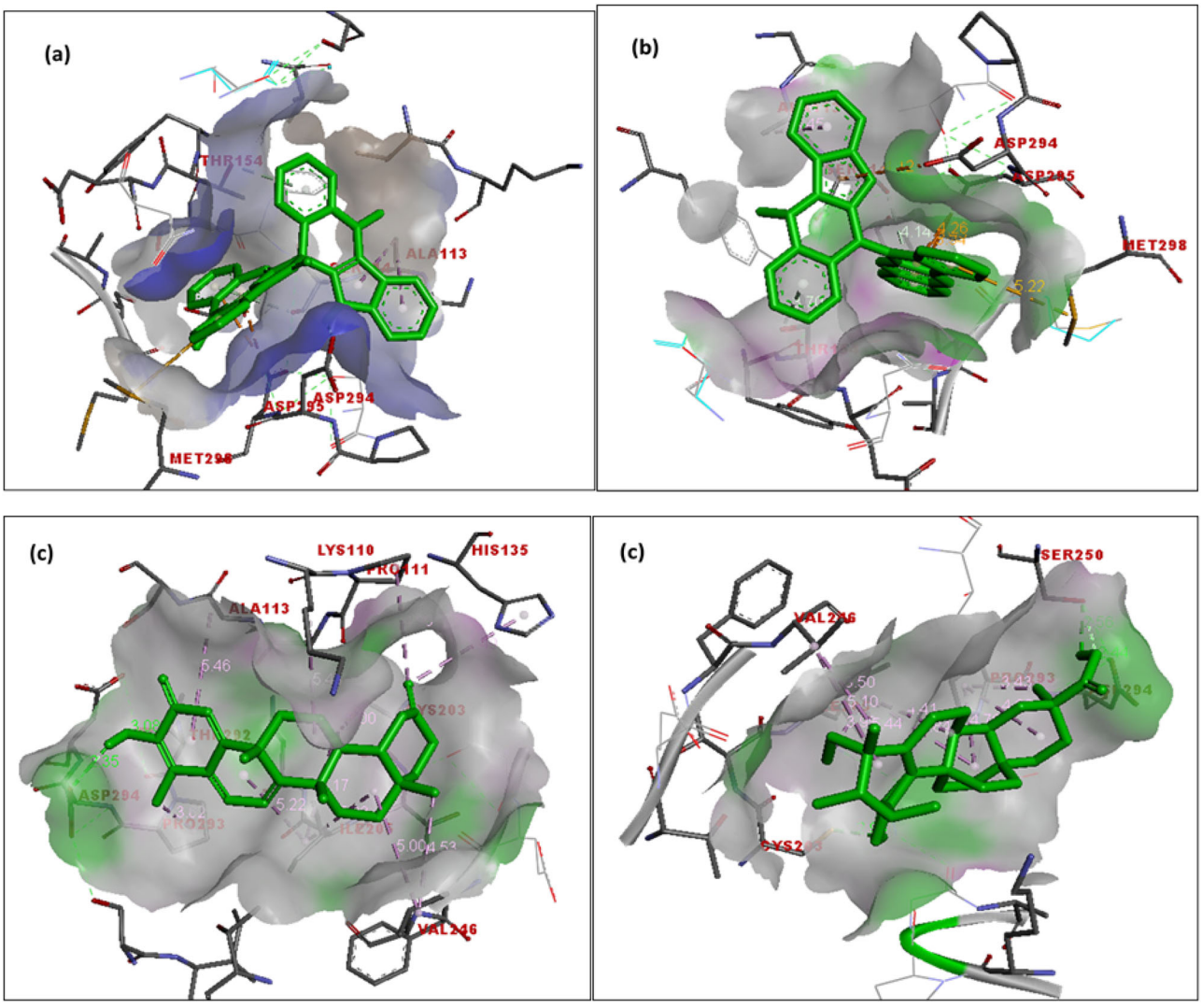

Figure 5. Visualization of MERS-CoV 3CL^{pro} amino acids interactions with ligands (a) Cryptospirolepine (b) Cryptoquindoline (c) Isoiguesterin (d) 20-*Epi*-isoiguesterinol.

were indicated to be non-carcinogenic, with very low acute toxicity and aqueous solubility of < 0. The gastrointestinal absorption index was indicated to be high for 10-hydroxyusambarensine and 6-oxoisoiguesterin but low for the other two compounds (Table 5).

4. Discussion

Potential anti-coronavirus therapies are classified based on their targets: action of the lead agent on the host immune system, host cells, or on the coronavirus itself. This study is focused on the inhibition of 3CL^{pro} as a therapeutic approach of inhibiting the replicative potential of coronaviruses; the protein is specific for the virus and its inhibition may not pose health threats to the host.

The identification and development of potent and efficacious chemical agents against coronavirus could be achieved via three strategies (Wu et al., 2020; Zumla et al., 2016): testing existing broad-spectrum of anti-virals (Chan et al., 2013); the use of known molecular databases to screen for agents that may have a therapeutic effect on coronavirus (de Wilde et al., 2014; Dyall et al., 2014); and the direct-based genomic information and pathological characteristics of different coronaviruses to develop new targeted drugs. Some peptides and small molecules have been reported so far, as inhibitors that target SARS-CoV 3CL^{pro} (Pillaiyar et al., 2016). Natural products such as alkaloids and terpenoids with antiviral, antimalarial, antibacterial, anti-inflammatory, and immunomodulatory activities could effectively interact with target such as 3CL^{pro} of SARS-CoV-2 (Chen et al., 2020), and be vital for the prevention and treatment of COVID-19.

A monomer of 3CL^{pro} has three domains: domain I (residues 8–101), domain II (residues 102–184), and domain III (residues 201–303); and a long loop (residues 185–200) connects domains II and III. The catalytic site of 3CLpro occupies the gap between domains I and II, and has a CysHis catalytic dyad (Cys145 and His41).The enzymatic activity of the 3CLpro resides in the catalytic dyad of Cys145 and His41 (Yang et al., 2003). Lopinavir and Ritonavir, the reference compounds used in this study are antiretroviral, protease inhibitors recommended for the treatment of SARS and MERS, which have similar mechanisms of action as HIV (Li et al., 2020).

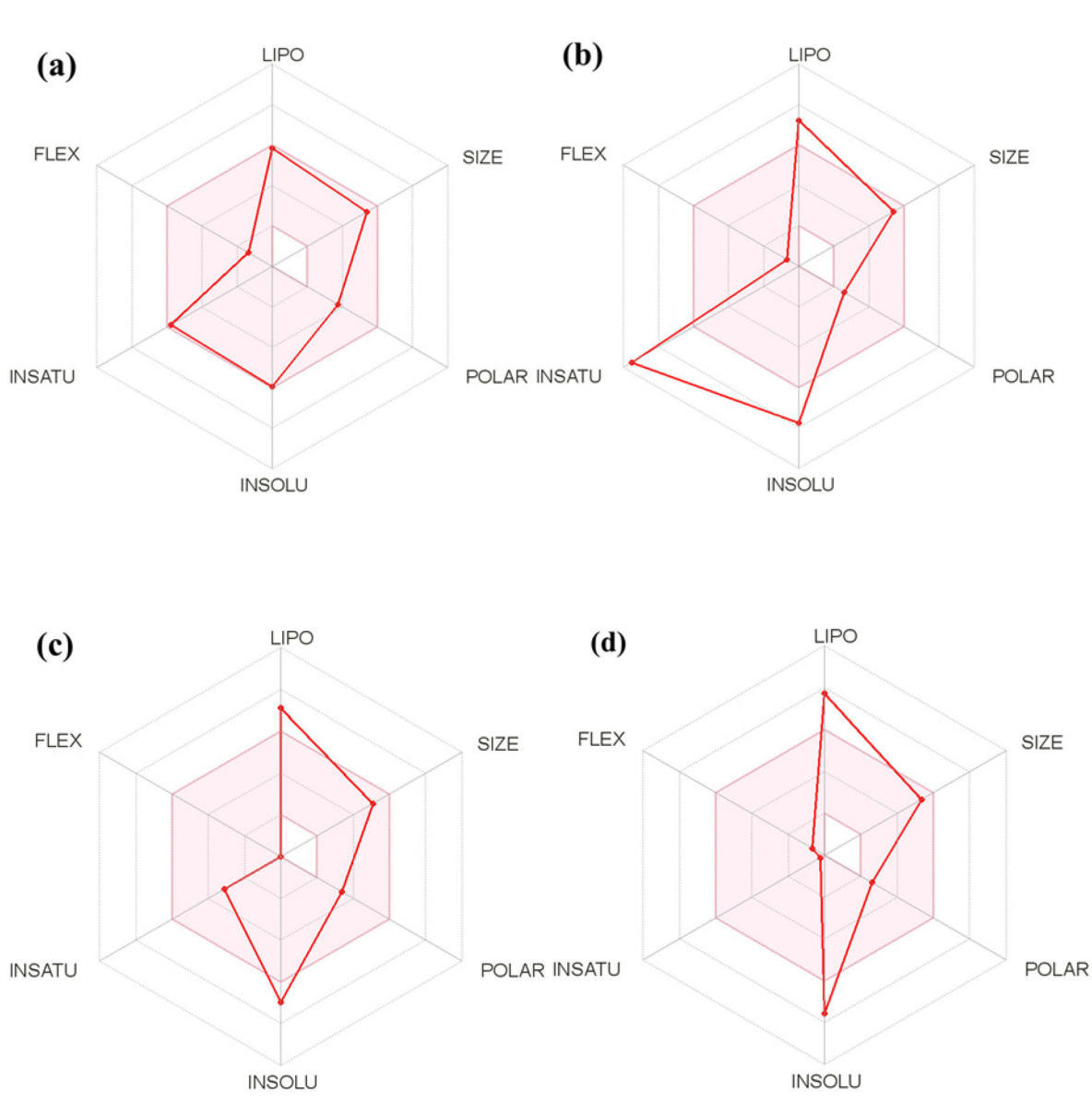

The colour space is the suitable physiochememical space for oral bioavailability
LIPO Lipophility: -0.7 < XLOGP3 < +5.0
SIZE: 150g/mol : < MW < 500g/mol
POLAR (Polarity): 20Å^2 < TPSA < 130 Å ^{2}
INSOLU (insolubility): 0 < Log S (ESOL) < 6
INSATU (insaturation): 0.25 < Fraction Csp3 <1
FLEX (Flexibity): 0 < Num. rotatable bonds < 9

Figure 6. Summary of phamacokinetic properties of top binding alkaloids and terpenoids from African plants to the 3CL^{pro} of SARS-Cov-2: (a) 10-hydroxyusambarensine, (b) cryptoquindoline, (c) 6-oxoisoiguesterin, (d) 22-hydroxyhopan-3-one.
The colour space is the suitable physiochememical space for oral bioavailability.
LIPO Lipophility: -0.7 < XLOGP3 < +5.0.
SIZE: 150g/mol : < MW < 500g/mol.
POLAR (Polarity): 20Å^2 < TPSA < 130 Å ^{2}.
INSOLU (insolubility): 0 < Log S (ESOL) < 6.
INSATU (insaturation): 0.25 < Fraction Csp3 < 1.
FLEX (Flexibity): 0 < Num. rotatable bonds < 9.

The top docked alkaloids and terpenoids with docking scores that surpassed that of the reference inhibitors suggests their promising efficacy as potential inhibitors of SARS-CoV-2 and the probable role of structural flexibility of interactions with the 3CL^{pro} of other coronaviruses (Sang et al., 2020).This binding is probably achieved by covalent

Table 4: Revalidation of the binding and docking properties of top docked compounds to respective proteins.

Bioactive compound	Interacted residues	Interacted residues involved in H-bonding (BOND DISTANCE)	Binding energy Kcal/mol	Poses in Cluster	Best Pose	Binding site coordinate
SARS-CoV-2						
Ritonavir	GLN^{189} GLU^{166} GLY^{143} MET^{49} MET^{165} PRO^{168}	GLY^{143} (2.61) GLU^{166} (2.81)	−7.0	95	181	−10.94, 12.98, 68.43
Lopinavir	GLN^{110} ASP^{153} SER^{158} ILE^{106} VAL^{104} PHE^{294} VAL^{297} PRO^{293} VAL^{202} ILE^{249}	GLN^{110} (2.11) ASP^{153} (2.80) SER^{158}(3.09)	−8.4	81	133	−38.75, 11.96, 5111
10 -Hydroxyusambarensine	GLN^{189} TYR^{54} MET^{49} MET^{165} HIS^{163} CYS^{145} GLU^{166} PRO^{168} HIS^{41} PHE^{140}	GLN^{189} (2.97) TYR^{54} (2.51)	−10.1	64	147	−11.34, 12.13, 69.13
Cryptoquindoline	CYS^{148} MET^{49} MET^{165} HIS^{41} PHE^{140} ASN^{142} GLN^{189}		"−9.70	56	26	−9.89, 13.66, 67.80
6-Oxoisoiguesterin	GLN^{189} MET^{49} MET^{165} $ASN^{142}$$HIS^{41}$		−9.10	67	142	−9.76, 15.40, 68.75
22-Hydroxyhopan-3-one	LYS^{137} LEU^{275} LEU^{287} LEU^{286} TYR^{239} THR^{199} TYR^{273}	LYS^{137} (3.16)	−8.70	65	168	−26.41, −6.36, 55.37
SARS-CoV						
10 -Hydroxyusambarensine	VAL^{104} ILE^{106} GLN^{110} LEU^{202} ILE^{249} PHE^{294} PRO^{252} THR^{292}		−10.10	74	106	56.09, −7.81, 27.36
Cryptospirolepine	MET^{49} GLU^{47} GLU^{166} THR^{25}	HIS^{41} (2.21)	−10.50	58	24	42.31, 12.60, 3.68
6-Oxoisoiguesterin	THR^{292} THR^{111} PRO^{252} PRO^{293} ILE^{294} PHE^{294} VAL^{297} GLN^{110} ASN^{151}	THR^{292} (3.30) THR^{111} (2.01) GLN^{110} (2.46) ASN^{151} (2.81)	−9.50	64	110	55.62, −8.30, 27.53
20-*Epi*-isoiguesterinol	THR^{24} THR^{25} ALA^{46} CYS^{145} HIS^{41} MET^{165}	THR^{24} (2.97) THR^{25}(2.92)	−9.3	58	24	42.99, 13.10, 3.81
MERS-CoV						
Cryptospirolepine	ASP^{294} THR^{154} THR^{292}	ASP^{294} (2.49) THR^{292} (3.13)	−10.90	78	308	9.50, 58.23, 30.81
Cryptoquindoline	MET^{6} THR^{154}		−9.70	68	116	8.53, 57.22, 28.19
Isoiguesterin	ASP^{294} THR^{292} ALA^{113} PRO^{293} $LYS^{110}$$HIS^{135}$ VAL^{246} PRO^{111} CYS^{203} ILE^{205}	ASP^{294} (2.35)THR^{292} (3.08)	−9.40	85	138	12.97, 55.41, 39.38
20-*Epi*bryonolic acid	ASP^{294} CYS^{203} SER^{250} PRO^{293} $ILE^{205}$$VAL^{246}$	ASP^{294} (2.94) CYS^{203} (2.56) SER^{250} (2.99)	−9.5	78	178	12.51, 56.11, 38.22

Table 5. Physicochemical properties of the top binding alkaloids and terpenoids from African plants.

(a) Lipinski filter analysis				
Lipinski filters	10 -Hydroxyusambarensine	Cryptoquindoline	6-Oxoisoiguesterin	22-Hydroxyhopan-3-one
Molecular weight (g/mol)	448.56	448.52	420.58	442.72
Num. heavy atoms	34	35	31	32
Num. rotatable bonds	2	1	0	1
Num. H-bond acceptors	3	2	3	2
Hydrogen bond donor	3	0	2	1
cLogP	3.31	4.02	4.80	4.41
Molar Refractivity	142.46	145.65	126.84	135.30
Lipinski violation	0	0	0	0
(b) admet SAR				
Absorption (Probability)				
Blood-Brain Barrier	BBB+ (0.83)	BBB+ (0.95)	BBB+ (0.53)	BBB+ (0.97)
Human Intestinal Absorption	HIA+ (0.98)	HIA+ (0.99)	HIA+ (0.99)	HIA+ (1.00)
Bioavailability Score	0.55	0.55	0.55	0.55
Caco-2 Permeability	Caco2+ (0.53)	Caco2+ (0.76)	Caco2+ (0.79)	Caco2+ (0.85)
P-glycoprotein Substrate	Substrate (0.91)	Non-inhibitor (0.69)	Non-inhibitor (0.77)	Substrate (0.54)
P-glycoprotein Inhibitor	Non-inhibitor (0.60)	Non-inhibitor (0.72)	Non-inhibitor (0.71)	Non-inhibitor (0.61)
Renal Organic Cation Transporter	Inhibitor (0.80)	Non-inhibitor (0.67)	Non-inhibitor (0.83)	Non-inhibitor (0.77)
Distribution (Probability)				
Subcellular localization	Mitochondria (0.65)	Mitochondria (0.55)	Mitochondria (0.89)	Mitochondria (0.53)
Metabolism				
CYP450 Substrate	Substrate (0.53) Non-inhibitor (0.83)	substrate Non-inhibitor (0.76)	Non-substrate (0.84) inhibitor (0.67)	Inhibitor (0.73) Non-substrate (0.63)
Toxicity				
AMES Toxicity	Non AMES toxic (0.75)	AMES toxic (0.89)	Non AMES toxic (0.91)	Non AMES toxic (0.87)
Carcinogens	Non-carcinogens (0.97)	Non-carcinogens (0.92)	Non-carcinogens (0.90)	Non-carcinogens (0.88)
Acute Oral Toxicity	III (0.51)	III (0.67)	III (0.63)	III (0.75)
Rat Acute Toxicity LD_{50}, mol/kg	2.7896	2.4420	2.0255	2.7443
Aqueous solubility (LogS)	−2.7626	−3.1120	−4.7201	−4.1004
Pharmacokinetics				
GI absorption	High	Low	High	low
Log K_p (skin permeation) cm/s	−5.70	−3.97	−3.93	−3.29

alteration of the thiolate anion of the active Cys residue (Berry et al., 2015) because most of the interactions involved the Cys residue. The antiviral activity of the alkaloids against coronaviruses is associated with the direct inhibition the $3CL^{pro}$ (Jo et al., 2020).

The binding affinity exhibited by 10-hydroxyusambarensine, cryptoquindoline, and cryptospirolepine (the top docked alkaloids) portrays the alkaloids to have strong binding tendency with inhibitory potential against $3CL^{pro}$ of SARS-CoV-2, SARS-CoV. While 10-hydroxyusambarensine exhibited the strongest interactions with $3CL^{pro}$ of SARS-CoV-2, cryptospirolepine exhibited highest binding affinity and selectivity for $3CL^{pro}$ of SARS-CoV and MERS-CoV. These compounds had higher docking scores, good binding affinities, and more interactions with the conserved catalytic dyad residues (Cys-145 and His-41) that are important for the catalytic function of the $3CL^{pro}$. These compounds also interacted with Asp^{187} know to enhance the catalytic efficiency of $3CL^{pro}$ (Zhao et al., 2008).

The comparison between the revalidated and vina result showed a consistency in binding affinities and binding pattern, also the binding site coordinate of the compounds in selected cluster as indicated by BINDSURF docking analysis further revalidate the docking of compounds onto the Cys-His catalytic dyad (Cys-145 and His-41) of the SARS-CoV-2 $3CLO^{pro}$.

The binding pattern of the top docked terpenoids was conserved between SARS-CoV-2 and SARS-CoV. The binding of 6-oxoisoiguesterin to the $3CL^{pro}$ of SARS-CoV-2 and SARS-CoV makes it a valuable compound against the viral activities of these coronaviruses. However, Isoiguesterin and 20-epi-bryonolic acid may be better inhibitors of the viral function of MERS-CoV $3CL^{pro}$ since they interacted with amino acid residue of the domain III. Domain III of 3CLpro is also proposed as a new target for specific inhibitors because of its critical importance in the function of the viral enzyme (Anand et al., 2003).

The better interactions of these terpenoids with $3CL^{pro}$ compared with that of reference compounds, suggest the terpenoids may alter the viral protease function essential for processing the viral replicase polyproteins. A series of diterpenoids have been identified as moderate competitive inhibitor of the $3CL^{pro}$. A structural activity relationship suggested the quinine-methide and hydrophobic E ring assists in producing the inhibitory activity (Pillaiyar et al., 2016). The results obtained in this study corroborate findings from similar studies in which the selected compounds were docked into the conserved catalytic dyad residues (Cys-145 and His-41), and interacted with receptor-binding residues Thr^{24}, Thr^{25}, Thr^{26}, Met^{49}, Asn^{142}, Cys^{44}, Thr^{45}, Ser^{46}, Gly^{143}, His^{164}, Glu^{166} and Gln^{189} (Ul Qamar et al., 2020).

The strikingly similar ligand-binding pattern exhibited by ritonavir, 10-hydroxyusambarensine, cryptoquindoline, 6-oxoisoiguesterin and 20-*Epi*-isoiguesterinol to the CysHis catalytic dyad (Cys145 and His41) and HIS163/HIS172/GLU166 indicates the conservation of the catalytic dyad across the two. The latter residues are believed to provide the opening gate for the substrate in the active site of the protome (Yang et al., 2003) of SARS-Cov-2 and SARS-CoV $3CL^{pro}$. This further reveals that SARS-Cov-2 receptor-binding pocket

conformation resembles that of the SARS-CoV $3CL^{pro}$ and raises the possibility that inhibitors intended for SARS-Cov-2 $3CL^{pro}$ may also inhibit the activity of SARS-CoV $3CL^{pro}$. The different binding pattern exhibited by $3CL^{pro}$ of MERS-CoV to its top docked ligands, in which most of them were docked into the cleft of domain III, is consistent with the findings that SARS-Cov-2 is more similar to SARS-CoV than MERS-CoV (Xu et al., 2020; Zhou et al., 2020; Zhu et al., 2020).

From the Lipinski and predicted ADME/tox filtering analyses, we identified four non-toxic, druggable natural compounds that bind to the receptor-binding site and catalytic dyad (Cys-145 and His-41) of SARS-CoV-2 $3CL^{pro}$. The four compounds (Table 4) which are potential drug candidates had no violation of Lipinski's rule. This accepted Rule-of-five defines the relationship physicochemical between and pharmacokinetics parameters (Lipinski, 2000). Lipinski's rule states that, generally, an orally active drug will not have more than one violation of the following criteria: Not >5 hydrogen bond donors (oxygen or nitrogen atoms with one or more hydrogen atoms); Not >10 hydrogen bond acceptors (nitrogen or oxygen atoms); A molecular mass <500 Daltons; and an octanol-water partition coefficient (log P) not greater than 5. The result from the predicted filtering analyses of the four compounds showed parameters that suggests a favourable ADME/tox and pharmacokinetic properties. This further indicates the druggability potential of the best docked alkaloids and terpenoids. This may be a pointer to a structure-based design of drugs that targets the $3CL^{pro}$ of SARS-CoV-2, and useful against COVID-19.

5. Conclusion

In conclusion, our study revealed that natural agents from the alkaloids and terpnoids class of compounds are capable of inhibiting the $3CL^{pro}$ with a highly conserved inhibitory pattern to both SARS-CoV-2 and SARS-CoV. Taken into account the site of inhibition, the strength of the binding affinity, the interaction with the conserved catalytic dyad residues (Cys-145 and His-41) and the favorable predicted ADME/tox parameters; 10-Hydroxyusambarensine, Cryptoquindoline, 6-Oxoisoiguesterin and 22-Hydroxyhopan-3-one may be potent against SARS-CoV-2 $3CL^{pro}$. Further experimental studies are suggested to check the possible preclinical and clinical efficacy of these agents for the prevention and treatment of COVID-19.

Disclosure statement

No potential conflict of interest was reported by the authors.

Funding

This study was not funded.

References

Aanouz, I., Belhassan, A., El Khatabi, K., Lakhlifi, T., El Idrissi, M., & Bouachrine, M. (2020). Moroccan Medicinal plants as inhibitors of COVID-19: Computational investigations. *Journal of Biomolecular Structure and Dynamics* (just-accepted), 1–12.

Amoa Onguéné, P., Ntie-Kang, F., Lifongo, L. L., Ndom, J. C., Sippl, W., & Mbaze, L. M. (2013). The potential of anti-malarial compounds derived from African medicinal plants, part I: A pharmacological evaluation of alkaloids and terpenoids. *Malaria Journal*, *12*, 449. https://doi.org/10.1186/1475-2875-12-449

Anand, K., Ziebuhr, J., Wadhwani, P., Mesters, J. R., & Hilgenfeld, R. (2003). Coronavirus main proteinase (3CLpro) structure: Basis for design of anti-SARS drugs. *Science (New York, N.Y.).)*, *300*(5626), 1763–1767. https://doi.org/10.1126/science.1085658

Berry, M., Fielding, B. C., & Gamieldien, J. (2015). Potential broad spectrum inhibitors of the coronavirus 3CLpro: A virtual screening and structure-based drug design study. *Viruses* , *7*(12), 6642–6660. https://doi.org/10.3390/v7122963

Boopathi, S., Poma, A. B., & Kolandaivel, P. (2020). Novel 2019 Coronavirus structure, mechanism of action, antiviral drug promises and rule out against its treatment. *Journal of Biomolecular Structure and Dynamics* (just-accepted), 1–14.

Cascella, M., Rajnik, M., Cuomo, A., Dulebohn, S. C., & Di Napoli, R. (2020). *Features, evaluation and treatment coronavirus (COVID-19). StatPearls [Internet]*. StatPearls Publishing.

Chan, J. F. W., Chan, K.-H., Kao, R. Y. T., To, K. K. W., Zheng, B.-J., Li, C. P. Y., Li, P. T. W., Dai, J., Mok, F. K. Y., Chen, H., Hayden, F. G., & Yuen, K.-Y. (2013). Broad-spectrum antivirals for the emerging Middle East respiratory syndrome coronavirus. *The Journal of Infection*, *67*(6), 606–616. https://doi.org/10.1016/j.jinf.2013.09.029

Chen, Y. W., Yiu, C.-P B., & Wong, K.-Y. (2020). Prediction of the SARS-CoV-2 (2019-nCoV) 3C-like protease (3CL (pro)) structure: Virtual screening reveals velpatasvir, ledipasvir, and other drug repurposing candidates. *F1000Research*, *9*, 129. https://doi.org/10.12688/f1000research.22457.1

Cheng, F., Li, W., Zhou, Y., Shen, J., Wu, Z., Liu, G., Lee, P. W., & Tang, Y. (2012). admetSAR: A comprehensive source and free tool for assessment of chemical ADMET properties. *Journal of Chemical Information and Modeling*, *52*(11), 3099–3105. https://doi.org/10.1021/ci300367a

de Wilde, A. H., Jochmans, D., Posthuma, C. C., Zevenhoven-Dobbe, J. C., van Nieuwkoop, S., Bestebroer, T. M., van den Hoogen, B. G., Neyts, J., & Snijder, E. J. (2014). Screening of an FDA-approved compound library identifies four small-molecule inhibitors of Middle East respiratory syndrome coronavirus replication in cell culture. *Antimicrobial Agents and Chemotherapy*, *58*(8), 4875–4884. https://doi.org/10.1128/aac.03011-14

Dong, E., Du, H., & Gardner, L. (2020). An interactive web-based dashboard to track COVID-19 in real time. *Lancet Infectious Diseases*. https://doi.org/10.1016/s1473-3099(20)30120-1

Dyall, J., Coleman, C. M., Hart, B. J., Venkataraman, T., Holbrook, M. R., Kindrachuk, J., Johnson, R. F., Olinger, G. G., Jahrling, P. B., Laidlaw, M., Johansen, L. M., Lear-Rooney, C. M., Glass, P. J., Hensley, L. E., & Frieman, M. B. (2014). Repurposing of clinically developed drugs for treatment of Middle East respiratory syndrome coronavirus infection. *Antimicrobial Agents and Chemotherapy*, *58*(8), 4885–4893. https://doi.org/10.1128/aac.03036-14

Elfiky, A. A., & Azzam, E. B. (2020). Novel Guanosine Derivatives against MERS CoV polymerase: An in silico perspective. *Journal of Biomolecular Structure and Dynamics*, (just-accepted), 1–12.

Elmezayen, A. D., Al-Obaidi, A., Şahin, A. T., & Yelekçi, K. (2020). Drug repurposing for coronavirus (COVID-19): In silico screening of known drugs against coronavirus 3CL hydrolase and protease enzymes. *Journal of Biomolecular Structure and Dynamics*, (just-accepted), 1–12.

Gupta, M. K., Vemula, S., Donde, R., Gouda, G., Behera, L., & Vadde, R. (2020). In-silico approaches to detect inhibitors of the human severe acute respiratory syndrome coronavirus envelope protein ion channel. *Journal of Biomolecular Structure and Dynamics*, 1–11. https://doi.org/10.1080/07391102.2020.1751300

Hasan, A., Paray, B. A., Hussain, A., Qadir, F. A., Attar, F., Aziz, F. M., & Mehrabi, M. (2020). A review on the cleavage priming of the spike protein on coronavirus by angiotensin-converting enzyme-2 and furin. *Journal of Biomolecular Structure and Dynamics*, (just-accepted), 1–13.

Jo, S., Kim, S., Shin, D. H., & Kim, M.-S. (2020). Inhibition of SARS-CoV 3CL protease by flavonoids. *Journal of Enzyme Inhibition and Medicinal Chemistry*, *35*(1), 145–151. https://doi.org/10.1080/14756366.2019.1690480

Khan, R. J., Jha, R. K., Amera, G., Jain, M., Singh, E., Pathak, A., & Singh, A. K. (2020). Targeting SARS-CoV-2: A systematic drug repurposing approach to identify promising inhibitors against 3C-like proteinase and 2′-O-ribosemethyltransferase. *Journal of Biomolecular Structure and Dynamics*, (just-accepted), 1–40.

Khan, S. A., Zia, K., Ashraf, S., Uddin, R., & Ul-Haq, Z. (2020). Identification of chymotrypsin-like protease inhibitors of SARS-CoV-2 via integrated computational approach. *Journal of Biomolecular Structure and Dynamics*, 1–10. https://doi.org/10.1080/07391102.2020.1751298

Lessene, G., Czabotar, P. E., Sleebs, B. E., Zobel, K., Lowes, K. N., Adams, J. M., Baell, J. B., Colman, P. M., Deshayes, K., Fairbrother, W. J., Flygare, J. A., Gibbons, P., Kersten, W. J. A., Kulasegaram, S., Moss, R. M., Parisot, J. P., Smith, B. J., Street, I. P., Yang, H., Huang, D. C. S., & Watson, K. G. (2013). Structure-guided design of a selective BCL-X(L) inhibitor. *Nature Chemical Biology*, *9*(6), 390–397. https://doi.org/10.1038/nchembio.1246

Li, J. Y., You, Z., Wang, Q., Zhou, Z. J., Qiu, Y., Luo, R., & Ge, X. Y. (2020). The epidemic of 2019-novel-coronavirus (2019-nCoV) pneumonia and insights for emerging infectious diseases in the future. *Microbes and Infection*, *22*(2), 80–85. https://doi.org/10.1016/j.micinf.2020.02.002

Lipinski, C. A. (2000). Drug-like properties and the causes of poor solubility and poor permeability. *Journal of Pharmacological and Toxicological Methods*, *44*(1), 235–249. https://doi.org/10.1016/S1056-8719(00)00107-6

Muralidharan, N., Sakthivel, R., Velmurugan, D., & Gromiha, M. M. (2020). Computational studies of drug repurposing and synergism of lopinavir, oseltamivir and ritonavir binding with SARS-CoV-2 Protease against COVID-19. *Journal of Biomolecular Structure and Dynamics*, (just-accepted), 1–7.

Ndhlala, A. R., Amoo, S. O., Ncube, B., Moyo, M., Nair, J. J., & Van Staden, J. (2013). Antibacterial, antifungal, and antiviral activities of African medicinal plants. In *Medicinal plant research in Africa* (pp. 621–659): Elsevier.

Nickel, J., Gohlke, B.-O., Erehman, J., Banerjee, P., Rong, W. W., Goede, A., Dunkel, M., & Preissner, R. (2014). SuperPred: Update on drug classification and target prediction. *Nucleic Acids Research*, *42*(Web Server issue), W26–31. https://doi.org/10.1093/nar/gku477

O'Boyle, N. M., Banck, M., James, C. A., Morley, C., Vandermeersch, T., & Hutchison, G. R. (2011). Open Babel: An open chemical toolbox. *Journal of Cheminformatics*, *3*, 33https://doi.org/10.1186/1758-2946-3-33

Osafo, N., Mensah, K. B., & Yeboah, O. K. (2017). Phytochemical and pharmacological review of *Cryptolepis sanguinolenta* (Lindl.) schlechter. *Adv Pharmacol Sci*, *2017*, 3026370https://doi.org/10.1155/2017/3026370

Pant, S., Singh, M., Ravichandiran, V., Murty, U., & Srivastava, H. K. (2020). Peptide-like and small-molecule inhibitors against Covid-19. *Journal of Biomolecular Structure and Dynamics*, (just-accepted), 1–15.

Pelz, N. F., Bian, Z., Zhao, B., Shaw, S., Tarr, J. C., Belmar, J., Gregg, C., Camper, D. V., Goodwin, C. M., Arnold, A. L., Sensintaffar, J. L., Friberg, A., Rossanese, O. W., Lee, T., Olejniczak, E. T., & Fesik, S. W. (2016). Discovery of 2-indole-acylsulfonamide myeloid cell leukemia 1 (Mcl-1) inhibitors using fragment-based methods. *J. Med. Chem*, *59*(5), 2054–2066. https://doi.org/10.1021/acs.jmedchem.5b01660

Pillaiyar, T., Manickam, M., Namasivayam, V., Hayashi, Y., & Jung, S. H. (2016). An overview of severe acute respiratory syndrome-coronavirus (SARS-CoV) 3CL protease inhibitors: Peptidomimetics and small molecule chemotherapy. *Journal of Medicinal Chemistry*, *59*(14), 6595–6628. https://doi.org/10.1021/acs.jmedchem.5b01461

Sanchez-Linares, I., Perez-Sanchez, H., Cecilia, J. M., & Garcia, J. M. (2012). High-Throughput parallel blind Virtual Screening using BINDSURF. *BMC Bioinformatics*, *13*(Suppl 14), S13. https://doi.org/10.1186/1471-2105-13-s14-s13

Sang, P., Tian, S., Meng, Z., Yang, L. (2020). Insight derived from molecular docking and molecular dynamics simulations into the binding interactions between HIV-1 protease inhibitor s and SARS-CoV-2 3CLpro. *Preprint*. https://chemrxiv.org/articles/Insight_Derived_from_Molecular_Docking_and_Molecular_Dynamics_Simulations_into_the_Binding_Interactions_Between_HIV-1_Protease_Inhibitors_and_SARS-CoV-2_3CLpro/11932995/1.

Sarma, P., Sekhar, N., Prajapat, M., Avti, P., Kaur, H., Kumar, S., & Dhibar, D. P. (2020). In-silico homology assisted identification of inhibitor of RNA binding against 2019-nCoV N-protein (N terminal domain). *Journal of Biomolecular Structure and Dynamics*, (just-accepted), 1–11.

Setzer, W. N., Holland, M. T., Bozeman, C. A., Rozmus, G. F., Setzer, M. C., Moriarity, D. M., Reeb, S., Vogler, B., Bates, R. B., & Haber, W. A. (2001). Isolation and frontier molecular orbital investigation of bioactive quinone-methide triterpenoids from the bark of *Salacia petenensis*. *Planta Medica*, *67*(1), 65–69. https://doi.org/10.1055/s-2001-10879

Souers, A. J., Leverson, J. D., Boghaert, E. R., Ackler, S. L., Catron, N. D., Chen, J., Dayton, B. D., Ding, H., Enschede, S. H., Fairbrother, W. J., Huang, D. C. S., Hymowitz, S. G., Jin, S., Khaw, S. L., Kovar, P. J., Lam, L. T., Lee, J., Maecker, H. L., Marsh, K. C., … Elmore, S. W. (2013). ABT-199, a potent and selective BCL-2 inhibitor, achieves antitumor activity while sparing platelets. *Nature Medicine*, *19*(2), 202–208. https://doi.org/10.1038/nm.3048

Trott, O., & Olson, A. J. (2010). AutoDock Vina: improving the speed and accuracy of docking with a new scoring function, efficient optimization, and multithreading. *Journal of Computational Chemistry*, *31*(2), 455–461. https://doi.org/10.1002/jcc.21334

Ul Qamar, M. T., Alqahtani, S. M., Alamri, M. A., & Chen, L.-L. (2020). Structural basis of SARS-CoV-2 3CLpro and anti-COVID-19 drug discovery from medicinal plants. *Journal of Pharmaceutical Analysis*. https://doi.org/10.1016/j.jpha.2020.03.009

Wang, M., Cao, R., Zhang, L., Yang, X., Liu, J., Xu, M., Shi, Z., Hu, Z., Zhong, W., & Xiao, G. (2020). Remdesivir and chloroquine effectively inhibit the recently emerged novel coronavirus (2019-nCoV) in vitro. *Cell Research*, *30*(3), 269–271. https://doi.org/10.1038/s41422-020-0282-0

Who, W.-C J. (2020). Report of the WHO-China Joint Mission on Coronavirus Disease 2019 (COVID-19). Geneva 2020.

Wu, C., Liu, Y., Yang, Y., Zhang, P., Zhong, W., Wang, Y., Wang, Q., Xu, Y., Li, M., Li, X., Zheng, M., Chen, L., & Li, H. (2020). Analysis of therapeutic targets for SARS-CoV-2 and discovery of potential drugs by computational methods. *Acta Pharmaceutica Sinica B*. https://doi.org/10.1016/j.apsb.2020.02.008

Xu, Z., Peng, C., Shi, Y., Zhu, Z., Mu, K., Wang, X., & Zhu, W. (2020). Nelfinavir was predicted to be a potential inhibitor of 2019-nCov main protease by an integrative approach combining homology modelling, molecular docking and binding free energy calculation. *BioRxiv*, *1*, 0–2.

Yang, H., Yang, M., Ding, Y., Liu, Y., Lou, Z., Zhou, Z., Sun, L., Mo, L., Ye, S., Pang, H., Gao, G. F., Anand, K., Bartlam, M., Hilgenfeld, R., & Rao, Z. (2003). The crystal structures of severe acute respiratory syndrome virus main protease and its complex with an inhibitor. *Proceedings of the National Academy of Sciences of the United States of America*, *100*(23), 13190–13195. https://doi.org/10.1073/pnas.1835675100

Zhao, Q., Li, S., Xue, F., Zou, Y., Chen, C., Bartlam, M., & Rao, Z. (2008). Structure of the main protease from a global infectious human coronavirus, HCoV-HKU1. *Journal of Virology*, *82*(17), 8647–8655. https://doi.org/10.1128/jvi.00298-08

Zhou, P., Yang, X.-L., Wang, X.-G., Hu, B., Zhang, L., Zhang, W., Si, H.-R., Zhu, Y., Li, B., Huang, C.-L., Chen, H.-D., Chen, J., Luo, Y., Guo, H., Jiang, R.-D., Liu, M.-Q., Chen, Y., Shen, X.-R., Wang, X., … Shi, Z.-L. (2020). A pneumonia outbreak associated with a new coronavirus of probable bat origin. *Nature*, *579*(7798), 270–273. https://doi.org/10.1038/s41586-020-2012-7

Zhu, N., Zhang, D., Wang, W., Li, X., Yang, B., Song, J., Zhao, X., Huang, B., Shi, W., Lu, R., Niu, P., Zhan, F., Ma, X., Wang, D., Xu, W., Wu, G., Gao, G. F., & Tan, W. (2020). A novel coronavirus from patients with pneumonia in China, 2019. *The New England Journal of Medicine*, *382*(8), 727–733. https://doi.org/10.1056/NEJMoa2001017

Zumla, A., Chan, J. F., Azhar, E. I., Hui, D. S., & Yuen, K. Y. (2016). Coronaviruses - drug discovery and therapeutic options. *Nature Reviews. Drug Discovery*, *15*(5), 327–347. https://doi.org/10.1038/nrd.2015.37